Solution Dynamics and Secondary Structure of Murine Leukemia Inhibitory Factor: A Four-Helix Cytokine with a Rigid CD Loop[†]

Duncan H. Purvis[‡] and Bridget C. Mabbutt*[,§]

School of Biochemistry and Molecular Genetics, University of New South Wales, Sydney NSW 2052, and MUCAB Protein Structure Group, School of Chemistry, Macquarie University, Sydney NSW 2109, Australia

Received March 21, 1997; Revised Manuscript Received June 9, 1997[⊗]

ABSTRACT: Leukemia inhibitory factor (LIF) is a hematopoietic cytokine which elicits its effects on diverse cell types via both gp130 and a more specific LIF receptor. Recombinant murine LIF was studied by multidimensional homonuclear and $^{1}H-^{15}N$ heteronuclear NMR and 95% of backbone amide resonances assigned. Definition of the secondary structure by chemical shift data and NOE connectivities shows a four-α-helix bundle fold (helices A−D) in solution, with an additional flexible turn of helix in the AB loop. Subtle differences are seen in the conformations of helices A and D from those defined in the crystal structure [Robinson, R. C., Grey, L. M., Staunton, D., Vankelcom, H., Vernallis, A. B., Moreau, J.-F., Stuart, D. I., Heath, J. K., & Jones, E. Y. (1994) *Cell 77*, 1101−1116]. The dynamics of the polypeptide backbone of LIF were assessed from ^{15}N T_1 and T_2 relaxation times and $^{15}N-^{1}H$ heteronuclear NOEs of the amide groups. Using model-free formalism, the overall rotational correlation time of LIF in solution is calculated to be 9.7 ps. The four α-helices are relatively rigid, and high mobility is observed for N-terminal residues (Ser 1−Asn 21) and the AB loop. In contrast to several closely related cytokines, the long CD loop is relatively rigid. This may have implications for interactions with the specific LIF receptor, which binds in this region.

Leukemia inhibitory factor (LIF)[1] was originally named for its inhibitory effects on a leukemic cell line and has since been shown to elicit pleiotropic effects on hepatocytes, adipocytes, neurons, and embryonic stem cells *in vitro* (Hilton, 1992; Bock et al., 1992). Female mice lacking a functional LIF gene cannot implant blastocysts (Stewart et al., 1992), while both sexes show a markedly lower population of hematopoietic stem cells in spleen and bone marrow (Escary et al., 1993). The powerful effects of LIF are mediated through two cell-surface receptor molecules, gp130 and LIF receptor (LIFR), which are believed to oligomerize in the presence of LIF (Gearing et al., 1992), and activate intracellular tyrosine kinases (Taga & Kishimoto, 1995). One or both of these receptors are also involved in the receptor complexes of the closely related cytokines oncostatin M (OSM) (Bruce et al., 1992), ciliary neurotrophic factor (CNTF), cardiotrophin-1 (CT-1), interleukin-6 (IL-6), and IL-11, leading to similar cellular responses in the presence of these different cytokines.

Murine LIF is 180 amino acids in length and is normally glycosylated *in vivo*, but is fully biologically active when unglycosylated (Gough et al., 1988; Gearing et al., 1989). A recent crystal structure of murine LIF at 2.0 Å (Robinson et al., 1994) has shown that LIF has a four-α-helix bundle fold comprising helices A to D in an up-up-down-down topology, homologous to the structures of growth hormone (GH) (Abdel-Meguid et al., 1987), CNTF (McDonald et al., 1995), OSM (Hoffman et al., 1996), and granulocyte colony stimulating factor (G-CSF) (Hill et al., 1993; Lovejoy et al, 1993; Zink et al., 1994). Of this family, structure/function relationships for human GH have been the most extensively studied, with crystal structures of both the free and receptor-bound cytokine determined (de Vos et al., 1992; Ultsch et al., 1994). The latter structure, together with mutagenesis studies (Cunningham & Wells, 1993), defined two separate sites on the GH molecule used for sequential interaction with its specific receptor. Residues at the higher affinity site, site 1, occur in helix A, the carboxyl-terminus of the D helix, and the AB loop. The lower affinity site, site 2, incorporates residues from both the A and C helices.

In contrast, LIF binds to a heterodimeric assembly of the receptor components LIFR and gp130. From site-directed mutagenesis, a third receptor-binding epitope has recently been identified on LIF (Hudson et al., 1996), in addition to the two defined from the paradigm GH:GHR complex. LIFR also binds at site 3, situated at one "end" of the bundle, which includes residues of the CD loop, a region previously postulated to determine the species specificity of the LIF:LIFR interaction (Owczarek et al, 1993).

[†] These studies were supported by a grant from the National Health and Medical Research Council of Australia, an Australian Research Council Research Fellowship (B.C.M.), and an Australian Post-graduate Award (D.H.P.).

* Author to whom correspondence should be addressed. Fax: 61 2 9850 8313; e-mail: bridget.mabbutt@mq.edu.au.

[‡] University of New South Wales.

[§] Macquarie University.

[⊗] Abstract published in *Advance ACS Abstracts,* August 1, 1997.

[1] Abbreviations: CNTF, ciliary neurotrophic factor; CT-1 cardiotrophin-1; DQ, double quantum; DQF-COSY, double quantum-filtered correlated spectroscopy; G-CSF, granulocyte colony stimulating factor; GH, growth hormone; GHR, growth hormone receptor; HMQC, heteronuclear multiple quantum coherence; HSQC, heteronuclear single quantum coherence; IL, interleukin; LIF, leukemia inhibitory factor; LIFR, leukemia inhibitory factor receptor; m, murine; NOE, nuclear Overhauser effect; NOESY, nuclear Overhauser effect spectroscopy; OSM, oncostatin M; R_{ex}, conformational exchange term; S^2, order parameter; T_1, longitudinal relaxation time, T_2, transverse relaxation time; τ_c, overall rotational correlation time; τ_{int}, correlation time for internal motions; TPPI, time proportional phase incrementation; TOCSY, total correlation spectroscopy; 2D, two dimensional; 3D, three dimensional.

S0006-2960(97)00665-X CCC: $14.00

With the use of ^{15}N-labeled protein, high-resolution NMR methods can be used to uniquely monitor solution dynamics of a protein structure at atomic level. This provides enhanced information concerning the conformation of sites utilized in protein/protein interactions. The solution dynamics of two four-α-helix bundle cytokines have previously been investigated. Both IL-4 (Redfield et al., 1992) and G-CSF (Werner et al., 1994; Zink et al., 1994) were found to possess rigid helices and highly mobile AB and CD loop regions. In order to compare the solution structure and dynamics of LIF with its related cytokines, we have expressed ^{15}N-labeled murine LIF for multidimensional heteronuclear NMR study. We report here the sequential assignment of the backbone resonances of mLIF, the definition of its secondary structure in solution, and details of the dynamics of the polypeptide backbone of the protein.

EXPERIMENTAL PROCEDURES

Sample Preparation. Recombinant mLIF was expressed as a glutathione-S-transferase fusion protein (containing a thrombin cleavage site) using the plasmid pGEX-2T:LIF (Smith & Johnson, 1988; gift of AMRAD, Melbourne) in *Escherichia coli* strain NM522, essentially as described previously (Gearing et al., 1989). For isotopic labeling of mLIF, bacteria were grown in shaker flasks using 2 L of M9 defined media (Sambrook et al., 1989) enriched with 1 g/L $^{15}NH_4Cl$ as the sole nitrogen source. At a cell density giving $OD_{600} > 1$ (1 cm path length), protein expression was induced with 50 μM isopropyl thio-β-galactoside for 4−7 h. Cells were lysed, and glutathione sepharose-4B (Pharmacia) (10 mL in 50 % v/v phosphate buffered saline) was stirred into the soluble cell fraction (2 h) to selectively bind the fusion protein product. Following cleavage with human thrombin (BioScientific, 500 NIH units) at 20 °C (4 h), pure mLIF was obtained by cation-exchange and reversed phase high performance liquid chromatography (Gearing et al., 1989). The sequence of recombinant murine LIF prepared by the above procedure differs from that of the native protein by an additional Gly (numbered −1) at the N-terminus.

NMR Spectroscopy. All NMR experiments were performed at 37 °C on samples of 1 mM LIF in deuterated sodium acetate (30 mM, pH 4.05) in 90% H_2O/10% ^2H_2O or 100% ^2H_2O. Most spectra were acquired on a Bruker DMX-600 spectrometer equipped with pulsed field gradients, with additional data obtained on Bruker DRX-500, AM-500, and AMX-600 spectrometers. Proton and nitrogen carrier frequencies were 4.74 ppm (spectral width 10.4 ppm) and 116.5 ppm (spectral width 28.0 ppm), respectively, except when the proton carrier frequency was placed at 7.60 ppm for acquisition (spectral width 4.16 ppm). Quadrature detection was achieved using TPPI (Marion & Wüthrich, 1983) for all experiments except the ^{15}N−^{1}H NOE measurement, which used the States method (States et al., 1982). The sizes of 3D acquisitions were 128−144 × 64−72 × 2K data points. Solvent presaturation during the recycle delay (1.4−1.2 s) was used for water suppression, except for the ^{15}N relaxation measurements. Heteronuclear experiments used GARP decoupling of ^{15}N (Shaka et al., 1985) during acquisition, and a nominal $1/4J_{NH}$ of 2.25 ms. The ^{1}H dimension was referenced to an internal standard of 1,4-dioxan (at 37 °C, $\delta = 3.754$ ppm), and the ^{15}N dimension was referenced to an external standard of 50% nitromethane/50% C^2HCl_3 (at 25 °C, $\delta = 379.6$ ppm) (Wishart & Sykes, 1994).

NOESY mixing times were 200 ms for the 2D homonuclear experiment (Macura et al., 1981), 100 ms or 200 ms for ^{15}N-edited NOESY-HSQC experiments (Kay et al., 1989a) and 100 ms for the HMQC-NOESY-HMQC experiment (Frenkiel et al., 1990). Relatively short spin lock periods were used in the TOCSY experiments to minimize loss of magnetization due to relaxation: clean MLEV-17 pulse trains (Griesinger et al., 1988) of 35−50 ms at 10 kHz field strength were used for 2D TOCSY (Braunschweiler & Ernst, 1983), and a 40.2 ms DIPSI-2 pulse sequence (Rucker & Shaka, 1989) was employed in the ^{15}N-edited TOCSY-HSQC experiment (Marion et al., 1989). The double quantum (DQ) experiment (Wokaun & Ernst, 1977) used 2 × 25 ms delays to generate multiple quantum coherence.

Relaxation Measurements. Measurement of T_1 and T_2 values for ^{15}N nuclei used the pulse sequences of Stone et al. (1992). A WATERGATE sequence (Sklenár et al., 1993) was incorporated into the last INEPT transfer for water suppression, with selective pulses at 30 kHz rf strength and $\tau = 100\ \mu$s, and two 2 ms pulsed field gradients (2 G cm^{-1}). T_1 experiments were performed with 10 relaxation delays T: T = 7, 52 (×2), 102, 150, 200, 400, 700, 1000 (×2), 1500, and 2000 ms. T_2 experiments were performed with 8 relaxation delays T: T = 4.32, 19.5 (×2), 34.7, 50.0, 73.9, 99.9, 149, and 200 ms. Steady-state ^{15}N−^{1}H NOE values were determined from spectra recorded in the presence and absence of 3 s of proton saturation. The measurements were performed in triplicate using a refocused HSQC pulse sequence with gradient coherence selection (Ross et al., 1993a,b). The recycle delays were 3.0 and 2.7 s for the T_1 and T_2 experiments, respectively.

Data Processing and Analysis. Spectra were processed and analyzed using the FELIX software package (BioSym MSI). Apodization was applied to all dimensions, most commonly as phase-shifted-skewed-sine-bell or Lorentzian-to-Gaussian functions. The first point of data acquired on AM or AMX spectrometers was linearly predicted. Linear prediction was used to extend data of ^{15}N relaxation and 3D experiments by 50−100% in the indirectly detected dimensions prior to apodization. Following processing, 3D matrices contained 256 × 128 × 512 real points, with the ^{15}N dimension most coarsely resolved. Chemical shifts were analyzed as $\Delta\delta$ values, where $\Delta\delta = \delta_{observed} - \delta_{rc}$, and δ_{rc} are the random coil chemical shift values of Wishart et al. (1995). T_1 and T_2 values were obtained by least-squares fitting of peak heights to single exponential decay functions (Palmer et al., 1992). The average uncertainties in the T_1 and T_2 relaxation times for resonances away from the N-terminus were 10.4 and 8.2%, respectively. The average experimental error in the NOE value derived from duplicate experiments was 0.04. Cross peak heights were used to determine the heteronuclear NOE in triplicate HSQC spectra. The 24 NOE values in excess of 0.824 (the theoretical maximum) due to systematic error or solvent exchange effects were not further scaled.

For amides that successfully fitted the ^{15}N T_1, T_2, and NOE relaxation data, modeling of molecular motion was carried out using the Modelfree program (Palmer et al., 1991; Stone et al., 1992), which assumes the "model-free" formalism of Lipari & Szabo (1982a,b). The T_1/T_2 ratio observed for residues known to occur in helices were initially used to calculate a correlation time of 10.2 ± 0.9 ns. The spectral density functions subsequently derived for each ^{15}N nucleus according to the equations of Kay et al. (1989b) included

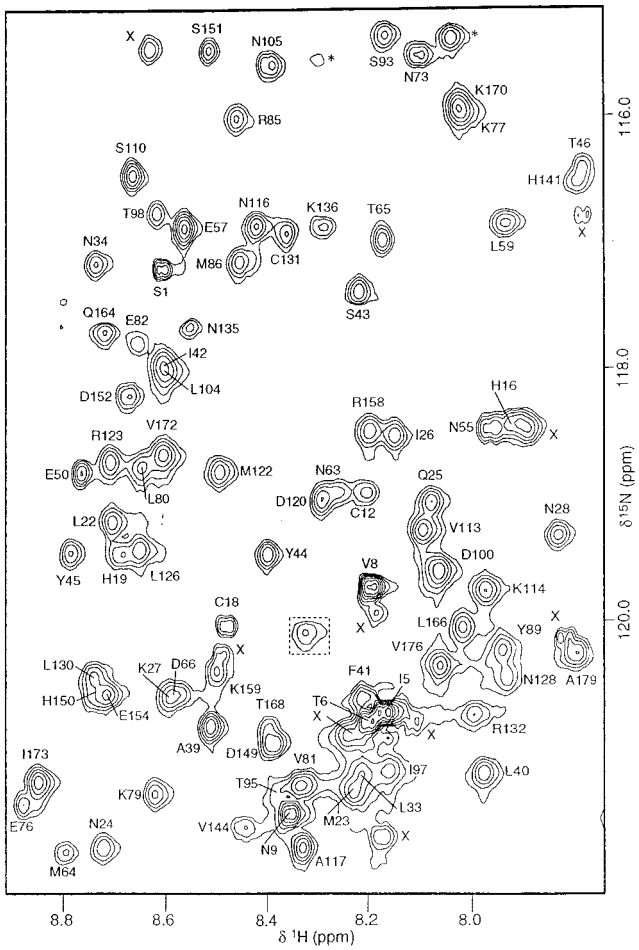

FIGURE 1: Region of the 2D $^{15}N-^{1}H$ HSQC of uniformly labeled mLIF (37 °C, pH 4.05, 600 MHz). Cross peaks from polypeptide amide resonances are well resolved and labeled according to their sequence assignments. Cross peaks denoted X are unassigned; * if from Gln or Asn side chains; boxed if from Arg side chain, folded into the spectrum.

terms for internal motions (τ_{int}) or exchange effects (R_{ex}), where they were significant at the 67% confidence level (Kördel et al., 1993). Uncertainties in order parameter values (S^2) averaged 8%. Calculation of the principal moments of inertia of mLIF was carried out using an in-house program (Dr Joel Mackay, personal communication).

RESULTS

NMR Assignments. The $^{15}N-^{1}H$ HSQC spectrum of LIF (Figure 1) shows well-dispersed cross peaks for all amide group resonances of this 19.9 kDa protein. The ^{1}H spin systems coupled to each amide resonance were identified from a 3D ^{15}N-edited TOCSY-HSQC experiment, as well as 2D TOCSY and DQF-COSY spectra (in $^{2}H_2O$). Distinctive ^{15}N chemical shift values were useful in confirming Gly, Thr, Ser, and Ala resonances (Wishart et al., 1995). The aromatic resonances of the six Tyr and six Phe residues in LIF were primarily identified from a 2D DQ spectrum in $^{2}H_2O$.

Sequential assignment (Wüthrich, 1986, Englander & Wand, 1987) relied on observation of inter-residue $d_{NN(i,i+1)}$ NOEs in the 3D ^{15}N-edited NOESY-HSQC (segments of which are shown in Figure 2). This type of connectivity is particularly strong for helical conformations and therefore favors the identification of sequences of residues in regions of α-helix. In cases where the HN resonances of sequential residues overlapped, the 3D HMQC-NOESY-HMQC experiment was particularly useful. NOEs due to $d_{\alpha N(i,i+1)}$ and $d_{\beta N(i,i+1)}$ connectivities confirmed assignments and indicated the direction of the sequence. The NOEs observed between resonances of sequential residues are shown in Figure 3 and allowed ^{1}H and ^{15}N resonances of 159 (i.e. 95%) of the 168 polypeptide backbone amide groups of mLIF to be assigned. Resonances of Ser 1 and Leu 3 were assigned, in the absence of inter-residue NOE connectivities, on the basis of their extremely long T_2 and large negative $^{15}N-^{1}H$ NOE values. The backbone amide resonances of Asn 21, Gln 29−Glu 32, Ser 36, Ser 69−His 71, and Val 147 remain unassigned. Aromatic ring resonances were sequence-specifically assigned from observation of intraresidue NOEs, or, in the case of phenylalanines 67, 52, 70, and 180, by identifying distinguishing long-range inter-residue NOEs consistent with the crystal structure of LIF (Robinson et al., 1994). Table 1S shows all chemical shift values of assigned resonances (Supporting Information).

Secondary Structure Determination. Distinctive intensities of NOEs due to sequential and medium-range (i.e. residues less than 5 apart) contacts (Wuthrich, 1986) were used to define the elements of secondary structure in mLIF. As the geometry of the polypeptide backbone is known to influence the chemical shift of $C^{\alpha}H$ and HN backbone resonances (Wishart et al., 1991), observed proton chemical shifts ($\Delta\delta$ values, summarized in Figure 4) were additionally used to delineate secondary structure: long sequential stretches of residues with negative $\Delta\delta$ values were defined to be in a helical conformation. The NOE and chemical shift parameters together essentially define four long helices for mLIF in solution: helices A (residues 22−48), B (76−103), C (109−135), and D (156−180). Two type I β-turns, involving residues Asn 105−Val 109 and His 150−Lys 153, are also defined by characteristic $d_{\alpha N(i,i+2)}$ NOE connectivities (seen in Figure 3).

The exact start of helix A is difficult to define in solution, although a helical conformation is clearly indicated for residues Leu 22−Asn 34 by the intensities of the sequential NOE connectivities (strong d_{NN}, weaker $d_{\alpha N}$ contacts) and chemical shifts (upfield shift of $C^{\alpha}H$ resonances). Helix A certainly is more stable from Gly 35 onward, however, as at this point additional medium-range contacts become evident. Within the AB loop, NOE connectivities in the segment Val 56−Cys 60 define an additional helix (denoted helix A′). Although this helix is too short to perturb the chemical shifts of the component $C^{\alpha}H$ atoms, from the mixture of medium-range contacts ($d_{\alpha N(i,i+2)}$ and $d_{\alpha N(i,i+4)}$, Figure 3) observed, it appears to be intrinsically flexible. Helix D is a relatively stable helix incorporating the C-terminal residue Phe 180, as a series of medium-range contacts link together the final segment of residues in the mLIF sequence.

The $\Delta\delta$ values for HN resonances of proteins, while generally dependent on solution conditions and subject to broad distribution, are also sensitive to helical structure through the helix dipole effect (Wishart et al., 1991). HN resonances of the residues at the N-terminus of an α-helix are shifted downfield while resonances of the C-terminal residues are shifted upfield. From the magnitude of $\Delta\delta$(HN) values observed for the helical residues of mLIF, this dipole effect is most obvious for resonances of helix B and least pronounced for helix A (Figure 4). In addition, a curved amphipathic α-helical peptide conformation has been proposed to cause $\Delta\delta$(HN) values to display a characteristic

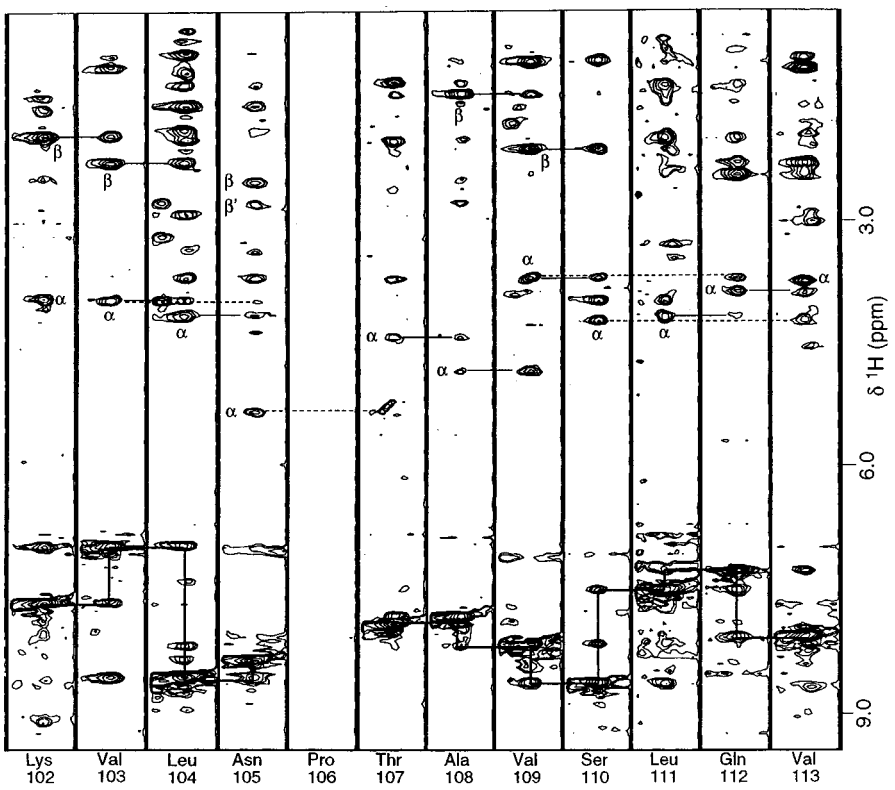

FIGURE 2: Strips from the 3D $^{15}N-^{1}H$ NOESY-HSQC spectrum of mLIF (37 °C, pH 4.05, 600 MHz) at the F_2 and F_3 frequencies of each NH resonance of sequential residues Lys 102−Val 113, which incorporates the BC loop region. The $C^{\alpha}H$ and $C^{\beta}H$ resonances coupled to each amide resonance are identified. Solid horizontal lines indicate sequential NOE connectivities, dotted lines indicate medium range $d_{\alpha N(i,i+2)}$ or $d_{\alpha N(i,i+3)}$ connectivities.

oscillation over three and four residues: positive for residues on the concave (inward) side of the helix, negative for those on the convex side (Zhou et al., 1992). This periodicity is readily observed in Figure 4 for the $\Delta\delta$(HN) values of residues in the long α-helices of mLIF, indicating that all four helices are smoothly curved. The effect is most distinct in helix B and occurs least in helix A. In this way, residues in the interior of each helix and therefore most likely to comprise the core of the helical bundle in solution are specifically identified: for example, Leu 80, Leu 83, Val 87, Ala 88, Ser 91, Leu 94, Thr 98, and Gln 101 from helix B, and Ser 110, Leu 115, Ile 119, Arg 123, Leu 126, Val 129, and Leu 133 from helix C.

Tertiary Fold of LIF in Solution. Collection of sufficient distance restraints to enable a tertiary structure calculation for mLIF is not possible using solely $^{15}N-^{1}H$ spectral information, because of the large number of signals and high degree of resonance overlap. Nevertheless, the tertiary fold of mLIF in solution can be coarsely defined from long-range NOE connectivities, using the well-resolved resonances of aromatic rings and methyl groups as structural probes. At this stage, several long-range contacts are observed linking Phe 41 with Gly 167, Phe 67 with Tyr 89, Phe 70 with Leu 83, Leu 80 with Phe 180, Tyr 84 with Val 129 and Leu 130, and Leu 126 with Val 87 and Ala 88. These side chain contacts allow definition of the tertiary fold of LIF as a four-α-helix bundle with up-up-down-down topology as depicted in Figure 5. The local solution environments mapped out around the side chains of aromatic residues by NOE contacts appear consistent with the molecular conformation depicted in the crystal structure of mLIF (Robinson et al., 1994). Absent in solution, however, is evidence of the medium to close-range contacts between Phe 180 and Phe 70 side chains. This may indicate some alteration from the crystalline conformation, or restricted solution mobility of either side chain.

The aromatic resonances of the Tyr 44 side chain are exchange-broadened at 37 °C, indicating restricted rotation and lower mobility relative to side chains of other Tyr residues in mLIF. Several NOEs are observed from these resonances to the polypeptide HN groups of residues 44, 45, and 163. We conclude that Tyr 44 is buried in the hydrophobic core of the protein, held rigidly in the same orientation as seen in the crystal structure. Preliminary NMR studies reporting the aromatic spin systems of human LIF and a murine-human chimeric molecule (Smith et al., 1994; Maurer et al., 1994) are very similar to those determined in this study, indicating that the aromatic ring environments in all three molecules are almost identical. Analysis of 2D NMR spectra recorded at different pH values (not shown) indicates that the three-dimensional structure of mLIF is fully conserved in solution over the pH range 3.0 to 6.9.

^{15}N Relaxation Measurements and Dynamics (model-free) Analysis. For well separated amide resonances, 125 T_1 curves, 132 T_2 curves, and 127 $^{1}H-^{15}N$ NOE values were defined. Derived ^{15}N relaxation parameters are graphed relative to amino acid sequence in Figure 6 and are analyzed in terms of the regions of secondary structure defined above for mLIF in solution (see Table 1). The relaxation time T_2 (or the ratio T_1/T_2) and NOE values are used here as sensitive experimental indicators of backbone dynamics.

The N-terminal residues of mLIF, from Ser 1 to Asn 21, have long T_2 relaxation times and negative NOE values, more typical of a highly mobile peptide than of a large rigid protein. Almost free motion is observed for Ser 1 to Thr 6. Two disulfide linkages anchoring Cys 12 and Cys 18 to the

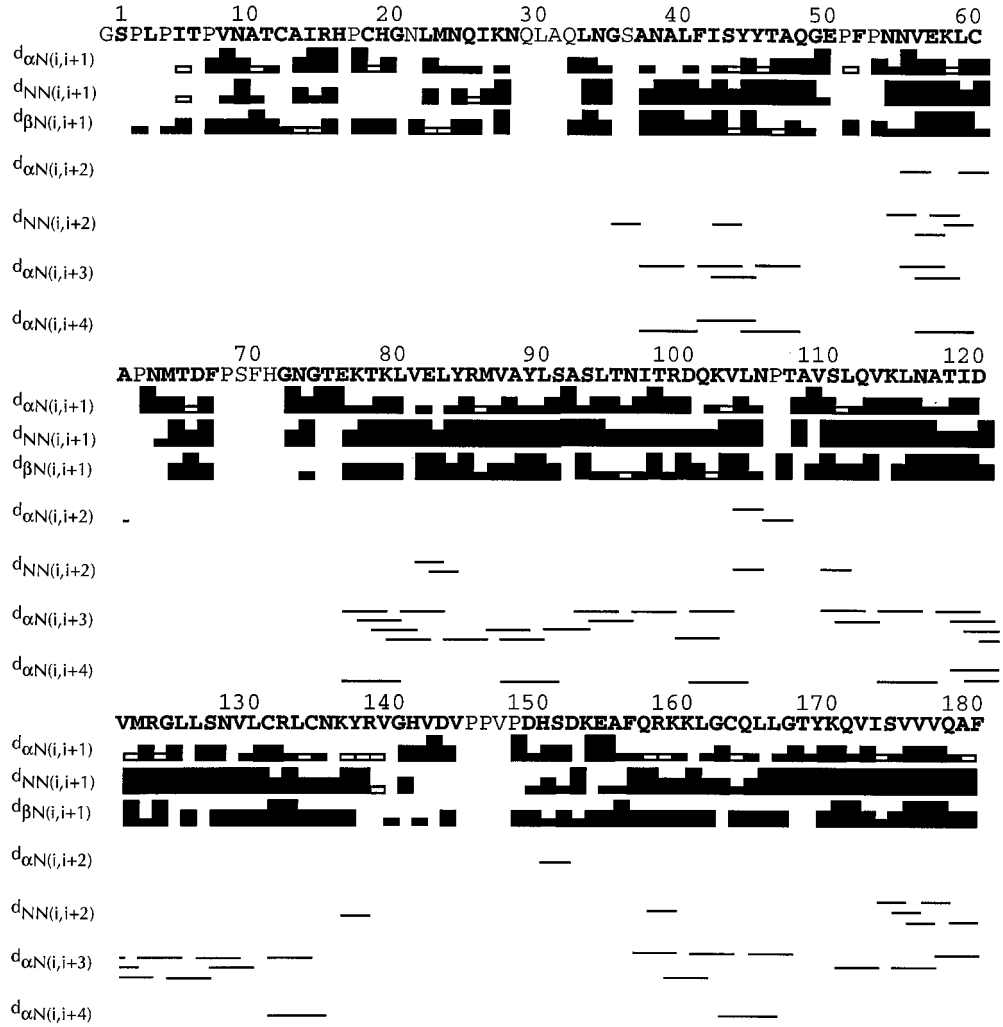

FIGURE 3: Summary of NOE connectivities observed between residues of mLIF. Sequential and medium range NOE connectivities observed in the 3D $^{15}N-^{1}H$ NOESY-HSQC spectrum (τ_m = 100 ms, 37 °C, pH 4.05, 600 MHz). Residues with assigned amide resonances are in bold type. For sequential connectivities (between residues *i* and *i*+1), NOEs were classified as strong, medium, or weak, and their approximate strength is indicated by the bar width. Hollow bars indicate ambiguous NOE strength due to resonance overlap. Medium range NOE connectivities are marked where present.

end of helix C (Nicola et al., 1993; Robinson et al., 1994) constrain this region somewhat, with Cys 12 preventing the very high mobility of residues 1−11 propagating further along the polypeptide chain.

Residues within the helices of the four-helix bundle characteristically possess shorter T_2 times (hence higher T_1/T_2 ratios) and higher NOE values than the surrounding segments. Helices B and C consistently show high NOE values (average 0.86), and helix A shows the highest average T_1/T_2 ratio (12.3). Relaxation parameters for helix D are also characteristic of a relatively rigid α-helix. No significant increase in T_2 or decrease in NOE values is seen toward the C-terminus of this helix, with the values for the C-terminal residue Phe 180 (T_2 = 82 ms, NOE = 0.85) being close to average for helix D. Residues forming the small helix A′ generally have low T_1/T_2 ratios and NOE values (average 9.2 and 0.78, respectively), indicating that this area is more flexible than the four long helices.

The AB loop region is characterized by consistently long T_2 times (average 96 ms) and low NOE values and is the most mobile region of the protein apart from the N-terminus. For this reason, some of the residues in this loop remain unassigned. The BC loop is very short and appears relatively constrained in mobility, with only a slightly lower average NOE (0.81) than the adjacent helical residues. Residues in the CD loop for which data is available also appear to be only of intermediate flexibility, with average values for T_1/T_2 ratio and NOE (9.4 and 0.79, respectively) close to those seen for the much shorter BC loop.

While the individual relaxation parameters described above qualitatively indicate the relative mobilities of different residues of mLIF in solution, a model-free analysis of measured T_1, T_2, and NOE values for 113 amide groups was carried out to derive quantitative parameters of the solution dynamics. For a ^{15}N nucleus relaxing solely through $^{15}N-^{1}H$ dipolar coupling and chemical shift anisotropy, the spectral density function is approximated by

$$J(\omega) = (S^2\tau_m)/[1 + (\omega\tau_m)^2] + (1 - S^2)\tau/[1 + (\omega\tau)^2]$$

where S^2 is an order parameter measuring the degree of restriction of motion, τ_m is the overall correlation time for the molecule, and $1/\tau = 1/\tau_m + 1/\tau_{int}$, where τ_{int} is the correlation time of rapid internal motions (Lipari & Szabo, 1982a,b).

The model-free analysis of relaxation properties generally assumes isotropic tumbling of the protein molecule. Using the crystal structure coordinates for mLIF (which do not include residues preceding Asn 9), the principal moments of inertia are determined to be in the ratio 2.4:2.3:1. In a

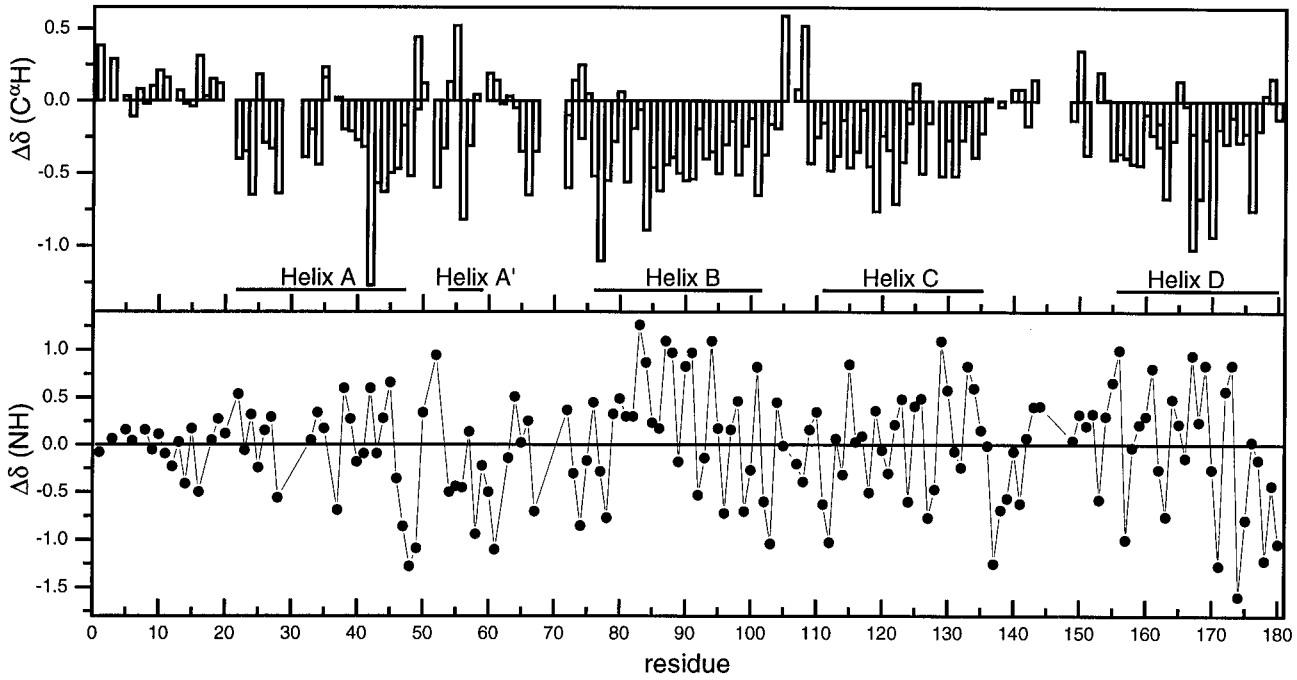

FIGURE 4: Proton chemical shifts (as $\Delta\delta$ values) for the $C^{\alpha}H$ and NH resonances of mLIF residues (37 °C, pH 4.05). $\Delta\delta = \delta_{observed} - \delta_{rc}$, where δ_{rc} are the random coil values of Wishart et al. (1995), i.e. a resonance shifted to higher field has a negative $\Delta\delta$ value. Black bars represent helical segments of mLIF identified from long runs of negative $\Delta\delta(C^{\alpha}H)$ values. Variations in $\Delta\delta$(NH) values reflect the dipole and amphipathicity of each helix.

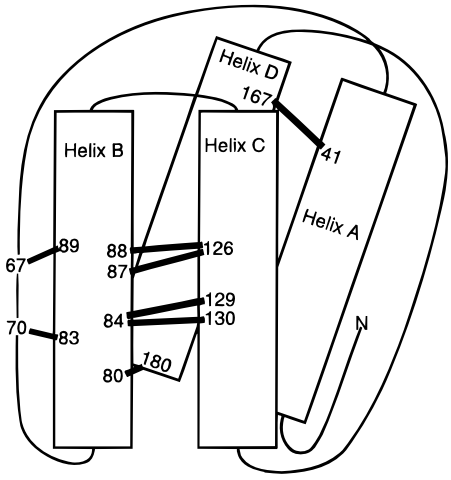

FIGURE 5: Schematic diagram of the solution topology of mLIF as defined by long-range NOE contacts. Helical regions are represented by white boxes, and black bars connect residues where NOE contacts have been observed in this work.

relaxation study of the related cytokine G-CSF, whose principal moments of inertia were in the ratio 2.1:1.8:1, Zink et al. (1994) found no significant differences in parameters derived from isotropic or anisotropic tumbling models. Given that the errors introduced by assuming isotropic tumbling for mLIF are therefore expected to be smaller than the experimental errors in the T_1/T_2 ratio, dynamics parameters for individual amide nuclei have been derived assuming isotropic molecular motion. The S^2 values calculated for amide groups of the mLIF polypeptide backbone are included in Figure 6 and Table 1.

The model-free analysis determined the global τ_c for mLIF at 37 °C to be 9.71 ± 0.08 ns. This value is close to global correlation times determined previously for other members of the four-helix cytokine family of proteins: 7.6 ns for human IL-4 at 35 °C (Redfield et al., 1992) and 12.1 ns for human G-CSF at 27 °C (Zink et al., 1994), which corresponds to 9.6 ns at 37 °C using the correction of Powers et al. (1992). Amide groups on the polypeptide backbone that display motion highly correlated with global tumbling typically have an order parameter $S^2 > 0.85$ (Clore et al., 1990). This is observed for amides of residues in helices B, C, and D of mLIF, indicating relative rigidity. Interestingly, such values are also seen for many residues comprising the CD loop. Significant motions of larger amplitude (i.e. $S^2 < 0.75$) are found clustered in three regions: the N-terminus, the AB loop, and the N-terminal half of helix A. The high mobility observed for residues at the start of helix A (Asn 28, Asn 34, and Leu 40 all have low S^2 values) may have contributed to our inability to assign the resonances of some residues in this region.

For 15 amide groups of mLIF, internal motion required a significant τ_{int} term (i.e. greater than the experimental uncertainty) in the spectral density function for modeling motion. Values obtained for τ_{int} ranged from 5.8 (Val 109) to 64 ps (Ala 10). Residues showing significant motion were clustered at the N-terminus, between Ala 10−Gly 20, and also in helix A′. The twelve residues whose mobility required a motional model including additional R_{ex} terms are distributed across the helices of mLIF, with a cluster of four in helix A between Asn 24−Asn 28. This possibly indicates a small amount of conformational exchange on the millisecond timescale. Such motions of the N-terminal half of helix A would explain the lack of medium-range NOEs connecting resonances of the helix A residues.

DISCUSSION

To our knowledge, mLIF is the largest protein to date for which NMR resonances have been assigned solely from uniformly ^{15}N-labeled protein samples. Murine LIF is here defined in solution as a relatively rigid four-α-helix bundle structure which extends from Leu 22 at the beginning of helix A to the C-terminal residue Phe 180 at the end of helix D, in an up-up-down-down topology. An additional helix

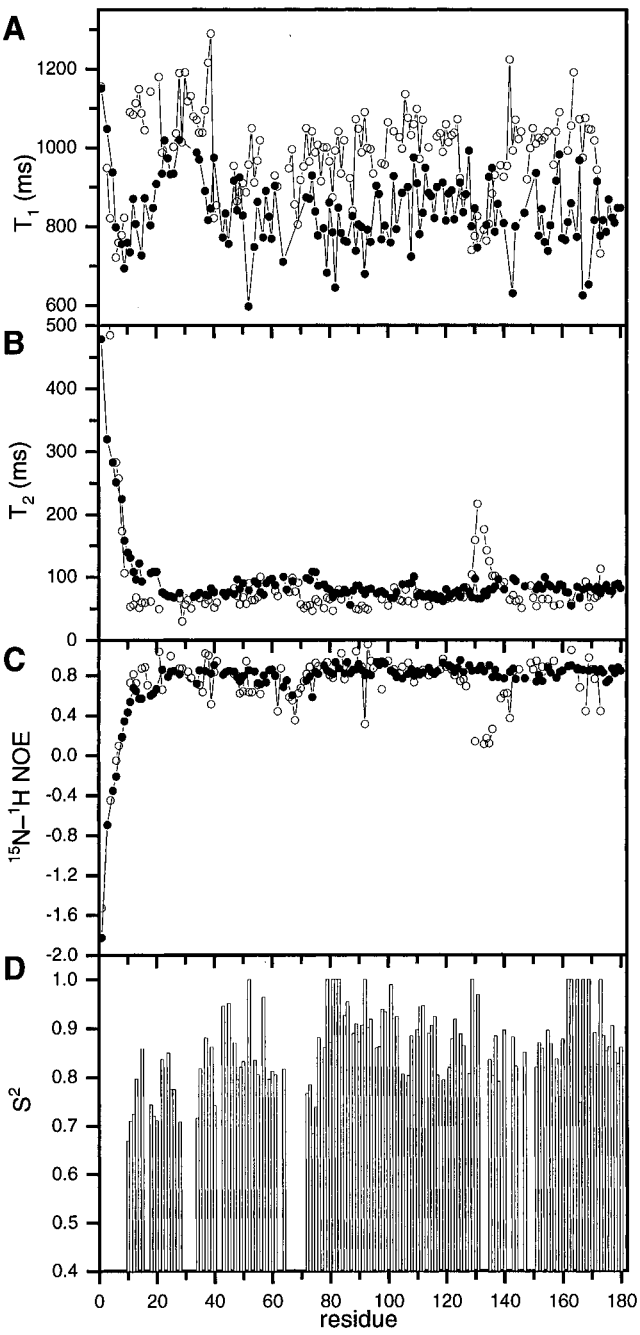

FIGURE 6: Experimental relaxation and solution dynamics parameters for ^{15}N-labeled mLIF (37 °C, pH 4.05). Plots show (A) ^{15}N T_1, (B) ^{15}N T_2, and (C) ^{15}N−^{1}H NOE values for each polypeptide amide resonance as closed circles. Analogous values for human G-CSF (at 27 °C) are shown as open circles (from Zink et al., 1994). (D) Order parameters, S^2, derived from model free analysis of mLIF relaxation.

A′ is seen as a flexible turn of helix between Val 56−Cys 60. The N-terminal region of the protein sequence, from Ser 1 to Gly 20, is highly mobile and unstructured in solution. All of the long α-helices forming the bundle are smoothly curved and relatively rigid. Helices B, C, and D all tumble rigidly within the overall molecular motion, with any internal motions of short duration. Helix A appears to be the least stable of the helices, with motions on several timescales (ps to ms) detected for residues within its N-terminal half. The AB loop is the only internal segment of the protein fold to show high mobility. The CD loop was found to exhibit only a slightly increased mobility relative to the helical regions of the protein.

Table 1: Relaxation Values and Model-Free Dynamics Parameters for Murine LIF (at 37 °C, pH 4.05)[a]

structural segment of mLIF	residues	T_2 (ms)	T_1/T_2	hNOE	S^2 value
N-terminus[b]	1−21	93−479	2.4−9.4	−1.82−0.68	0.74 ± 0.06[d]
helix A	22−48	74 ± 6	12.3 ± 1.6	0.82 ± 0.04	0.83 ± 0.08
A′ region[c]	49−60	86 ± 9	9.2 ± 1.4	0.78 ± 0.06	0.85 ± 0.08
AB loop	61−75	96 ± 10	8.6 ± 1.1	0.72 ± 0.09	0.77 ± 0.05
helix B	76−104	76 ± 7	10.3 ± 1.3	0.86 ± 0.05	0.92 ± 0.06
BC loop	105−108	85 ± 7	9.4 ± 1.2	0.81 ± 0.04	0.83 ± 0.05
helix C	109−135	75 ± 11	11.7 ± 1.6	0.86 ± 0.04	0.88 ± 0.07
CD loop	136−155	88 ± 7	9.4 ± 1.6	0.79 ± 0.05	0.85 ± 0.04
helix D	156−180	80 ± 8	10.4 ± 1.9	0.84 ± 0.04	0.89 ± 0.08

[a] Values quoted are means ± one standard deviation for the residues comprising the distinct secondary structure elements of mLIF as defined by this study. [b] A range of values, rather than the mean, is quoted where appropriate for the N-terminal residues. [c] The A′ region incorporates residues between the end of helix A and the end of helix A′. [d] These values for residues Ala 10−Gly 20 only.

Comparison with the Crystal Structure of mLIF. The molecular structure outlined here for mLIF in solution is generally in close agreement with the three-dimensional crystal structure (Robinson et al., 1994). We detect subtle differences in conformation, however, at the start of helix A, which in solution is smoothly curved and appears to lack some of the rigidity of a conventional α-helix, and also at the end of helix D, which shows α-helical character right up to the C-terminus in solution, but not in the crystalline form.

Mobility, or disorder, of the protein molecule in the crystalline state is partially reflected in the *B* factors derived for the electron density during crystallographic refinement. Across most of the mLIF fold, high *B* factors (Robinson et al., 1994) are observed in locations also defined as highly mobile from our solution relaxation parameters: the N-terminal residues Asn 9−Asn 21 have the highest *B* factors in the molecule; *B* factors are high at the start of helix A, probably due to some conformational heterogeneity; residues in the AB loop (Ser 69−Thr 75) have *B* factors > 30 Å^2; the CD loop contains some atoms with *B* factors close to 30 Å^2; residues in the short helix A′ do not have *B* factors any lower than those in surrounding sections. A difference is, however, again observed between solution and crystalline states at the C-terminus: atoms at the C-terminal end of helix D have gradually increased *B* factors, whereas the T_2 relaxation times seen in solution are more typical of a region of low mobility.

Comparison with the Structure and Dynamics of Other Cytokines. The structure of LIF shows that it is most closely related to members of the "long" four-α-helix bundle cytokine family: G-CSF (Hill et al., 1993; Werner et al., 1994; Zink et al., 1994), OSM (Hoffman et al., 1996), and CNTF (McDonald et al., 1995). In analogy to this study of mLIF, the solution dynamics have previously been defined in detail for human G-CSF. Figure 6 compares the measured dynamics parameters of murine LIF (at 37 °C) with those for human G-CSF (27 °C) (Zink et al., 1994). Altered solvent viscosity due to the temperature difference causes somewhat shorter T_1 and longer T_2 values for LIF. It is clear, however, that LIF and G-CSF share a similar pattern of solution dynamics: helices of low mobility, and an exceptionally mobile N-terminal region. The AB loop exhibits increased mobility to the same degree in both proteins, particularly at the C-terminal sections. The significant

difference in dynamics between the two proteins occurs in the CD loop. In G-CSF, the loop region containing Ala 129−Ser 142 is highly mobile, with heteronuclear NOE values close to zero, while the corresponding residues of mLIF (His 141−Glu 154) show only a slight decrease in NOE values from those of the neighboring helices. A large difference is also evident from the substantial variation in T_2 values of resonances of these residues. Certainly, no mobility on the scale of that seen for the CD loop of human G-CSF is observed for any residues comprising the mLIF helical bundle.

The dynamics of human IL-4 have also been studied in solution, at 35 °C (Redfield et al., 1992). This cytokine is a member of the "short" four-α-helix family, possessing 129 residues and two short β-strands in the AB and CD loops. Despite the difference in size, it is possible to directly compare the average order parameters between residues of both proteins. In both mLIF and IL-4, helix A was observed to be the most mobile (i.e. have low S^2 values) of the four rigid helices, and the most mobile regions of the protein are the N-terminus and the AB loop. Again, however, the CD loop of IL-4 is markedly more mobile than the same region in mLIF. In IL-4, the mobility of this loop (average $S^2 = 0.73$) is similar to that of the AB loop (average $S^2 = 0.65$).

Receptor Binding Sites of LIF. Three spatially distinct receptor epitopes have been defined for mLIF as a result of structure/function and site-directed mutagenesis studies (Owczarek et al., 1993; Layton et al., 1994; Hudson et al., 1996). Site 3 is the high-affinity site for the specific receptor component, LIFR; a second, low-affinity, site for LIFR binding corresponds to site 1 of hGH, and site 2 is the binding site for gp130, the commonly-shared cytokine receptor component. The solution dynamics of mLIF defined by this NMR study provide information on the mobility of these three receptor binding regions.

Residues at the N-terminus or at the end of the AB loop are the most mobile sections of mLIF and do not appear to contribute to receptor binding. The observation in solution of α-helical conformation to the very end of helix D may be important in contributing to the stability of site 1 for LIFR binding. Some residues of the AB loop also form part of this site, however, which is therefore the most mobile of the putative receptor binding regions of mLIF. The gp130 binding site (site 2) is formed from residues in helix A, which shows significant motions on the millisecond timescale, as well as the less mobile helix C. The major LIFR binding site (site 3) contains residues of the short BC loop, the end of the CD loop, and the start of helix D. All of these residues occur in regions of low mobility. In particular, the CD loop is unusually rigid in solution, and includes a β-turn at its C-terminus (His 150−Lys 153).

The rigid CD loop that contributes to binding site 3 of LIF appears to be an exception in the four-helical bundle family of cytokines. Of the LIFR-binding members of the family, OSM has a CD loop with a long, extended conformation in solution (Hoffman et al., 1996) and the CNTF X-ray crystal structure shows high disorder in this region (McDonald et al., 1995). Both of these cytokines bind to LIFR with low affinity, possibly also via a homologous site 3. Thus, the observed higher affinity of LIF for LIFR may be mediated through specific interactions that are enhanced by a rigid CD loop.

ACKNOWLEDGMENT

We thank Connie Akratos and Kathleen Curran for expression of a ^{15}N-labeled sample, Alfred Ross for supplying the ^{15}N−^{1}H NOE pulse program and helpful discussions, Joel Mackay for calculation of the moments of inertia of LIF, and AMRAD and Nicos Nicola for supplying the expression plasmid and help with LIF expression and purification. Thanks to Arthur Palmer, Brian Sykes, and David Wishart for making software available.

SUPPORTING INFORMATION AVAILABLE

Table 1S showing ^{1}H and ^{15}N NMR assignments for LIF at 37 °C, in 30 mM sodium acetate, pH 4.05, and Table 2S giving the values and errors of the experimentally determined ^{15}N relaxation data, together with derived model-free dynamics parameters for LIF (S^2, τ_{int}, R_{ex}) (16 pages). Ordering information is given on any current masthead page.

REFERENCES

Abdel-Meguid, S. S., Shieh, H.-S., Smith, W. W., Dayringer, H. E., Violand, B. N., & Bentle, L. A. (1987) *Proc. Natl. Acad. Sci. U.S.A. 84*, 6434−6437.

Bock, G. R., Marsh, J., & Widdows, K. (1992) *Polyfunctional Cytokines: IL-6 and LIF*, John Wiley & Sons, New York.

Braunschweiler, L., & Ernst, R. R. (1983) *J. Magn. Reson. 53*, 521−528.

Bruce, A. G., Linsley, P. S., & Rose, T. M. (1992) *Prog. Growth Factor Res. 4*, 157−170.

Cunningham, B. C., & Wells, J. A. (1993) *J. Mol. Biol. 234*, 554−563.

Clore, G. M., Driscoll, P. C., Wingfield, P. T. and Gronenborn, A. M. (1990) *Biochemistry 29*, 7387−7401.

de Vos, A. M., Ultsch, M., & Kossiakoff, A. A. (1992) *Science 255*, 306−312.

Englander, S. W., & Wand, A. J. (1987) *Biochemistry 26*, 5953−5958.

Escary, J.-L., Perreau, J., Duménil, D., Ezine, S., & Brûlet, P. (1993) *Nature 363*, 361−364.

Frenkiel, T., Bauer, C., Carr, M. D., Birdsall, B., & Feeney, J. (1990) *J. Magn. Reson. 90*, 420−425.

Gearing, D. P., Nicola, N. A., Metcalf, D., Foote, S., Wilson, T. A., Gough, N. M., & Williams, R. L. (1989) *Biotechnology 7*, 1157−1161.

Gearing. D. P., Comeau, M. R., Friend, D. J., Gimpel, S. D., Thut, C. J., McGourty, J., Brasher, K. K., King, J. A., Gillis, S., Mosley, B., Ziegler, S. F., & Cosman, D, (1992) *Science 255*, 1434−1437.

Gough, N. M., Hilton, D. J., Gearing, D. P., Willson, T. A., King, J. A., Nicola, N. A., & Metcalf, D. (1988) *Blood Cells 14*, 431−442.

Griesinger, C., Otting, G., Wüthrich, K., & Ernst, R. R. (1988) *J. Am. Chem. Soc. 110*, 7870−7872.

Hill, C. P., Osslund, T. D., & Eisenberg, D. (1993) *Proc. Natl. Acad. Sci. U.S.A. 90*, 5167−5171.

Hilton, D. J. (1992) *Trends Biochem. Sci. 17*, 72−76.

Hoffman, R. C., Moy, F. J., Price, V., Richardson, J., Kaubisch, D., Frieden, E. A., Krakover, J. D., Castner, B. J., King, J., March, C. J., & Powers, R. (1996) *J. Biomol. NMR 7*, 273−282.

Hudson, K. R., Vernallis, A. B., & Heath, J. K. (1996) *J Biol. Chem. 271*, 11971−11978.

Kay, L. E., Marion, D. E., & Bax, A. (1989a) *J. Magn. Reson. 57*, 404−426.

Kay, L. E., Torchia, D. A., & Bax, A. (1989b) *Biochemistry 28*, 8972−8979.

Kördel, J., Skelton, N. J., Akke, M., Palmer, A. G., III, & Chazin, W. J. (1993) *Biochemistry 31*, 4856−4866.

Layton, M. J., Owczarek, C. M., Metcalf, D., Clark, R. L., Smith, D. K., Treutlein, H. R., & Nicola, N. A. (1994) *J. Biol. Chem. 269*, 29891−29896.

Lipari, G & Szabo, A. (1982a) *J. Am. Chem. Soc. 104*, 4546−4559.

Lipari, G & Szabo, A. (1982b) *J. Am. Chem. Soc. 104*, 4559−4570.
Lovejoy, B., Cascio, D., & Eisenberg, D. (1993) *J. Mol. Biol. 234*, 640−653.
Macura, S., Huang, Y., Suter, D., & Ernst, R. R. (1981) *J. Magn. Reson. 43*, 259−281.
Marion, D., & Wüthrich, K. (1983) *Biochem. Biophys. Res. Commun. 113*, 967−974.
Marion, D., Kay, L. E., Sparks, S. W., Torchia, D. A., & Bax, A. (1989) *J. Am. Chem. Soc. 111*, 1515−1517.
Maurer, T., Smith, D. K., Owczarek, C. M., Layton, M. J., Zhang, J.-G., Nicola, N. A., & Norton, R. S. (1994) *Growth Factors 11*, 271−276.
McDonald, N. Q., Panayotatos, N., & Hendrickson, W. A. (1995) *EMBO J. 14*, 2689−2699.
Nicola, N. A., Cross, B., & Simpson, R. J. (1993) *Biochem. Biophys. Res. Commun. 190*, 20−26.
Owczarek, C. M., Layton, M. J., Metcalf, D., Lock, P., Willson, T. A., Gough, N. M., & Nicola, N. A. (1993) *EMBO J. 12*, 3487−3495.
Palmer, A. G., III, Rance, M., & Wright, P. E. (1991) *J. Am. Chem. Soc. 113*, 4371−4380.
Palmer, A. G., III, Cavanagh, J., Byrd, R. A., & Rance, M. (1992) *J. Magn. Reson. 96*, 416-424.
Powers, R., Garrett, D. S., March, C. J., Frieden, E. A., Gronenborn, A. M., & Clore, G. M. (1992) *Biochemistry 31*, 4334−4346.
Redfield, C., Boyd, J., Smith, L. J., Smith, R. A. G., & Dobson, C. M. (1992) *Biochemistry 31*, 10431−10437.
Robinson, R. C., Grey, L. M., Staunton, D., Vankelcom, H., Vernallis, A. B., Moreau, J.-F., Stuart, D. I., Heath, J. K., & Jones, E. Y. (1994) *Cell 77*, 1101−1116.
Ross, A. R., Czich, M., Cieslar, C., & Holak, T. A. (1993a) *J. Biomol. NMR 3*, 215−224.
Ross, A. R., Czich, M., Zink, T., & Holak, T. A. (1993b) *J. Magn. Reson. Series B 102*, 314-316.
Rucker, S. P., & Shaka, A. J. (1989) *Mol. Phys. 68*, 509−517.
Sambrook, J., Fritsch, E. F., & Maniatis, T. (1989) *Molecular Cloning: A Laboratory Manual*, Cold Spring Harbor Laboratory Press, Cold Spring Harbor.
Shaka, A. J., Barker, P. B., & Freeman, R (1985) *J. Magn. Reson. 64*, 547−552.
Sklenár, V., Piotto, M., Leppik, R., & Saudek, V. (1993) *J. Magn. Reson. Ser. A 102*, 241−245.
Smith, D. B., & Johnson, K. S. (1988) *Gene 67*, 31−40.
Smith, D. K., Treutlein, H. R., Maurer, T., Owczarek, C. M., Layton, M. J., Nicola, N. A., & Norton, R. S. (1994) *FEBS Letts. 350*, 275−280.
States, D. J., Haberkorn, R., & Ruben, D. J. (1982) *J. Magn. Reson. 48*, 286−292.
Stewart, C. L., Kaspar, P., Brunet, L. J., Bhatt, H., Gadi, I., Köntgen, F., & Abbondanzo, S. J. (1992) *Nature 359*, 76−79.
Stone, M. J., Fairbrother, W. J, Palmer, A. G., III, Reizer, J., Saier, M. H., Jr., & Wright, P. E. (1992) *Biochemistry 31*, 4394−4406.
Taga, T., & Kishimoto, T. (1995) *Curr. Opin. Immunol. 7*, 17−23.
Ultsch, M. H., Somers, W., Kossiakoff, A. A., & de Vos, A. M. (1994) *J. Mol. Biol. 236*, 286−299.
Werner, J. M., Breeze, A. L., Kara, B., Rosenbrock, G., Boyd, J., Soffe, N., & Campbell, I. D. (1994) *Biochemistry 33*, 7184−7192.
Wishart, D. S., Sykes, B. D., & Richards, F. M. (1991) *J. Mol. Biol. 222*, 311−333.
Wishart, D. S., & Sykes, B. D. (1994) *Methods Enzymol. 239*, 363−392.
Wishart, D. S., Bigam, C. G., Holm, A., Hodges, R. S., & Sykes, B. D. (1995) *J. Biomol. NMR 5*, 67−81.
Wokaun, A., & Ernst, R. R. (1977) *Chem. Phys. Lett. 52*, 407−412.
Wüthrich, K. (1986) *NMR of Proteins & Nucleic Acids*, J. Wiley, New York.
Zhou, N. E., Zhu, B.-Y., Sykes, B. D., & Hodges, R. S. (1992) *J. Am. Chem. Soc. 114*, 4320−4326.
Zink, T., Ross, A., Lüers, K., Cieslar, C., Rudolph, R., & Holak, T. A. (1994) *Biochemistry 33*, 8453−8463.

BI970665M